NASA Technical Memorandum 84320

Numerical Simulation of Turbulent Fluid Flows

A. Leonard

February 1983

National Aeronautics and
Space Administration

NASA Technical Memorandum 84320

Numerical Simulation of Turbulent Fluid Flows

A. Leonard, Ames Research Center, Moffett Field, California

National Aeronautics and
Space Administration

Ames Research Center
Moffett Field, California 94035

NUMERICAL SIMULATION OF FLUID FLOWS

A. Leonard

Ames Research Center

ABSTRACT

Recent developments in the numerical simulation of turbulent flows are discussed. This limited survey covers computational requirements for the direct simulation of turbulence, simulation of arbitrary homogeneous flows, a new expansion technique for wall-bounded flows with application to pipe flow, and possibilities of flow representations or modeling techniques that allow the simulation of high-Reynolds-number flows with a relatively small number of dependent variables.

INTRODUCTION

The numerical simulation of turbulent flows has a short history. Around 1950 von Neumann [1] and Emmons [2] proposed an attack on the turbulence problem by numerical simulation. But one could point to a beginning 20 years later in 1970-71 when Deardorff [3] reported on a large-eddy simulation of turbulent channel flow on a $24 \times 20 \times 14$ mesh and a direct simulation of homogeneous, isotropic turbulence was accomplished on a 32^3 mesh by Orszag and Patterson [4]. Perhaps the arrival of the CDC 6600 triggered these initial efforts. Since that time a number of developments have occurred along several fronts. Of course, faster computers with more memory continue to become available and it appears that this trend will not let up at least for another 3-5 years. In addition, new algorithms have been developed which extend or improve capabilities in turbulence simulation. For example, the simulation of arbitrary homogeneous flows and the efficient simulation of wall-bounded flows are now possible. Finally, the prospects for simulating high-Reynolds-number flows with limited computational resources have been realized with the development of subgrid-modeling techniques and vortex methods. As a result of all these developments, applications of turbulence simulation have been increasing rapidly in the past few years and will continue to do so.

In this paper I present examples of these new developments and discuss prospects for future developments.

PROBLEM OF NUMERICAL SIMULATION

We consider an incompressible flow whose time evolution is given by the Navier-Stokes equations for the velocity, $\underline{u}(\underline{x},t)$, and the pressure, $p(\underline{x},t)$, as

$$\frac{\partial \underline{u}}{\partial t} + \underline{u} \cdot \nabla \underline{u} = -\nabla p + \nu \nabla^2 \underline{u} \ , \tag{1a}$$

$$\nabla \cdot \underline{u} = 0 \ , \tag{1b}$$

along with appropriate initial and boundary conditions. It is assumed that the density = 1. The character of the solution depends on the Reynolds number of the flow, $Re = UL/\nu$, where U and L are a characteristic velocity and length of the large scale and ν is the kinematic viscosity. For small Reynolds numbers, one obtains a laminar flow that is smoothly varying in space and time; for large Reynolds numbers, one obtains a turbulent flow. Turbulent flows have been described as random, chaotic, vortical,

three-dimensional, and unsteady, and they are known to contain a wide range of scales. It is the combination of all these attributes that makes the numerical simulation of such flows extremely challenging.

In turbulent pipe flow, for example, we estimate, according to universal equilibrium theory [5], the smallest important scale of turbulence to be proportional to the dissipation, or Kolmogorov, length, $\eta = (\nu^3/\varepsilon)^{1/4}$, where ε is the energy-dissipation rate per unit mass, and the largest important scale to be some multiple of the pipe diameter. Using the volume-averaged ε given by

$$\varepsilon = -\frac{4\bar{U}\nu}{D}\left.\frac{\partial U}{\partial r}\right|_{wall} ,$$

where $\bar{U}$ is the mean velocity and D is the pipe diameter, we find that

$$\eta = \frac{(2/f)^{1/4}D}{Re^{3/4}} ,$$

where $Re = \bar{U}D/\nu$ and f is the friction factor,

$$f = 8(u_\tau/\bar{U})^2 ,$$

and u_τ is the wall shear velocity given by

$$u_\tau^2 = -\nu\left.\frac{\partial U}{\partial r}\right|_{wall} .$$

The friction factor, given implicitly by the formula [6],

$$\sqrt{\frac{8}{f}} = 2.44\ \ell n\left(\sqrt{\frac{f}{32}}\,Re\right) + 2.0 ,$$

is only weakly dependent on Reynolds number so that the required number of mesh points on a three-dimensional grid would be proportional to $(D/\eta)^3 \propto Re^{9/4}$. Figure 1 shows the energy spectrum measurements of Laufer [7] for high-Reynolds-number (Re = 500,000) pipe flow. The pipe diameter is 25.4 cm. The wave number corresponding to the Kolmogorov length, $k_\eta = 2\pi/\eta$, is seen to be well beyond the measured data. To simulate reliably the dissipation of turbulence energy, the grid spacing must be somewhat smaller than the length scale corresponding to the peak in the dissipation spectrum. If isotropy of the small scales is assumed the dissipation spectrum is proportional to $k_1^2E_1(k_1)$. In Laufer's experiment this peak, away from the wall, corresponds to a length of 150η or $0.03D$. Lawn's experiments [8] with lower Reynolds numbers (Re = 37,000 to 250,000) and those of Bakewell and Lumley [9] (Re = 8,700) indicate that the location of the peak dissipation scales on diameter (i.e., occurs at ~0.03D), not on Kolmogorov length. (It would appear that these Reynolds numbers are too low for universal equilibrium theory to apply. Nevertheless, I will assume that the Kolmogorov length is still a good measure of the smallest turbulent scale.) Thus, at low Reynolds numbers, the Kolmogorov wave number is much closer to the peak of the dissipation spectrum. For example, if Re = 5,000 the dissipation peak would correspond to a length of $\approx 7\eta$.

Therefore, as an estimate of the mean spacing between grid points, Δ, required in the direct simulation of turbulent pipe flow, we take $\Delta = 2\eta$. Table 1 gives corresponding estimates of the number of mesh points required for several Reynolds numbers, assuming that the computational domain extends 10 diameters in the streamwise direction. (This estimate could be off by a factor of 3 either way. Some measurements and their interpretation suggest correlation lengths of $20D$, others correlation lengths of $2D$; see Coles [10].) It appears that only the lowest Reynolds number case is accessible to present day supercomputers (10^8 floating point operations per second, 10^7 words storage).

In addition it should be verified that the spacing $\Delta = 2\eta$ is sufficiently small to allow resolution of all important turbulence phenomena near the wall. The grid spacing measured in wall units is given by

$$\Delta^+ = 2\eta^+$$

$$= 2\,\frac{\eta u_\tau}{\nu}$$

$$= 2\left(\frac{fRe}{32}\right)^{1/4} .$$

For Re from 5,000 to 500,000, Δ^+ ranges from 3.2 to 7.6 (see table 1). This spacing should provide sufficient resolution to reproduce all important wall-layer structures (such as streamwise streaks), which have characteristic lengths of 50-100 wall units. See Moin [11] for further discussion of this point.

The number of time-steps, Ns, required to follow one realization for a time T and obtain reasonable statistics also depends on Reynolds number. The time-step Δt is roughly limited to

$$\Delta t \le \frac{\Delta}{\bar{U}} .$$

Using the above estimate for Δ and $(2/f)^{1/4} \approx 3$ we find that

$$\Delta t \le \frac{6D}{\bar{U}Re^{3/4}} .$$

And if $T = 100\ D/U$, then

$$Ns = \frac{T}{\Delta t} \ge 17Re^{3/4} ,$$

or 10,000 steps for $Re = 5{,}000$.

DIRECT SIMULATION OF TURBULENCE

Homogeneous flows:

Probably the most ambitious direct simulations of turbulent flows to date are the computations of a variety of homogeneous turbulent flows by Rogallo [12] on a 128^3 mesh. Rogallo writes the velocity field $\underline{u}$ as the sum of a mean component and a turbulent component,

$$\underline{u} = \underline{U} + \underline{u}' ,$$

and assumes that the components of $\underline{U}$ have the form

$$U_m = U_{mn}(t)x_n ,$$

where repeated indices are summed. By transforming to coordinates, $\tilde{\underline{x}}$, moving with the mean flow he obtains momentum and continuity equations for $\underline{u}'$ that contain no explicit dependence on $\underline{x}$. Then Rogallo assumes that the turbulent component of the homogeneous flow is periodic in $\tilde{x}$-space, with period L_m in direction m; therefore, no further boundary conditions are required, and spatial derivatives can be computed accurately by Fourier interpolation. Thus, $\underline{u}'(\tilde{\underline{x}},t)$ is represented by

$$\underline{u}'(\tilde{\underline{x}},t) = \sum_{\underline{k}} \hat{\underline{u}}(\underline{k},t)e^{i\underline{k}\cdot\tilde{\underline{x}}} .$$

Here the mth component of k is

$$k_m = \pi\ell/L_m$$

and ℓ ranges over $-N/2 + 1 \le \ell \le N/2 - 1$, where $N = 128$ for Rogallo's simulations

and the Navier-Stokes equations become a $3(N-1)^3$ system of ordinary differential equations (ODEs),

$$\frac{d\hat{u}_m}{dt} + ik_n\widehat{u_m u_n} = \frac{ik_m k_\ell k_n \widehat{u_\ell u_n}}{k^2} - \nu k^2 \hat{u}_m \ ,$$

where $k^2 = k_n k_n$, and

$$\widehat{u_m u_n}(\underline{k}) = \sum_{\underline{k}'} \hat{u}_m(\underline{k}')\hat{u}_n(\underline{k} - \underline{k}') \ .$$

(In the above, zero mean flow, $U_{mn} = 0$, has been assumed in order to simplify the presentation.) To avoid explicit evaluation of the convolution sums $\widehat{u_m u_n}$ requiring $O(N^6)$ operations per step, fast Fourier transforms (FFTs) are used to return to physical space where the required products are formed and then transformed (by FFTs) back to Fourier space. Consequently, only $O(N^3 \log N)$ operations per step are required.

Suppose the tensor U_{mn} is decomposed into a symmetric (strain, R) and antisymmetric (vorticity, Ω) tensors; then the only constraint on R is that it be traceless $R_{nn} = 0$, but the vorticity must satisfy the evolution equation

$$\dot{\Omega}_{mn} + R_{mk}\Omega_{kn} + \Omega_{mk}R_{kn} = 0 \ .$$

Rogallo simulated four flows: plain strain, $U_{22} = -U_{33} = \text{const}$; axisymmetric strain, $U_{22} = U_{33} = -(1/2)U_{11} = \text{const}$; shear, $U_{12} = \text{const}$; and rotation, $U_{13} = -U_{31} = \text{const}$.

Figure 2 shows the energy spectrum and the component spectra for the case of homogeneous shear, $s = U_{12}$ at several dimensionless times, st, after starting from an isotropic field at $st = 0$. Note that at the small scales (large k) the component energies are nearly equally distributed, whereas the streamwise component (E_1) has the highest large-scale energy, and the shear-direction component (E_2) has the least. Figure 3 shows the tendency of the nondimensional turbulence energy to decrease and then equilibrate. All these features of the simulation are in agreement with experiment.

Agreement with experiment is of course desirable and provides confidence in the solutions but is not the ultimate goal of these simulations. New information about turbulent flows or new insights into the nature of turbulence is the desired outcome. For example, in the development of turbulence models, one hypothesizes relations between higher-order/multipoint moments of the velocity field and lower-order/single-point moments. Any desired statistics are readily computed from numerical simulations so that various hypotheses may be tested or new ones may suggest themselves. This is demonstrated in figure 4. The correlation between ϕ_{ij} — the sum of the slow pressure strain term (cubic in turbulence velocities) and the deviator of the dissipation tensor — and the energy tensor b_{ij}, given by

$$b_{ij} = \frac{u_i' u_j'}{q^2} - \frac{1}{3}\delta_{ij} \ ,$$

$$q^2 = u_j' u_j' \ ,$$

is shown in figure 4a. The correlation, suggested by the work of Lumley and Newman [13], is seen to be very good for the simulations of homogeneous shear and represents a significant improvement over earlier attempts to correlate the total pressure strain with the energy tensor. If ϕ_{ij} is modeled as

$$\phi_{ij} = \beta b_{ij}$$

and β is adjusted separately for each field to minimize the square error of the fit, then one obtains very good agreement of the model with measured values of ϕ_{ij}, as shown in figure 4b. In addition, Rogallo found that the adjusted values of β correlate well

with Reynolds number, R_L, as shown in figure 4c. (It can be shown analytically that $\beta \to 2$ as $R_L \to 0$.) Thus, the model above for ϕ with $\beta = \beta(R_L)$ is very promising.

Wall-bounded shear flows:

The direct simulation of wall-bounded shear flows presents a new set of difficulties because of the presence of the wall. Part of the problem is due to the physical processes near the wall. The thin shear layer next to the wall is continually breaking up via three-dimensional (3-D) inertial instabilities resulting in a violent 3-D wrinkling of the vortex layer. In the spanwise direction, the scale of the breakup is of the order of the thickness of the layer or tens of wall units and, perhaps, somewhat more in the streamwise direction.

Another part of the problem is algorithmic and is due to the no-slip boundary condition at the wall. One can no longer use Fourier series for the spectral expansion in the direction normal to the wall. Rather, to obtain rapid convergence independent of boundary constraints, one should employ global polynomials related to the eigenfunctions of a singular Sturm-Liouville problem [14]. Chebyshev and Legendre polynomials are popular choices but, as shown below in the case of pipe flow, other choices may be preferable because of special conditions of the problem at hand. Whatever the choice may be, this change in basis functions complicates the imposition of the no-slip condition and the satisfaction of the continuity constraint. These two conditions become global constraints on the expansion which are generally difficult or costly to impose simultaneously. By contrast, in the simulation of homogeneous flows using Fourier expansions in all three directions, the boundary conditions are built into the expansion and the divergence-free constraint is satisfied by a simple projection which is local in wavenumber space.

In the following, I shall describe a new technique for overcoming the algorithmic difficulties described above, at least for wall-bounded flows in simple geometries. The technique consists of expanding the velocity field in terms of a set of divergence-free vector functions satisfying the boundary conditions. First we write the Navier-Stokes equations in rotational form:

$$\frac{\partial \underline{u}}{\partial t} + \underline{\omega} \times \underline{u} = -\nabla\left(p + \frac{1}{2}\,u^2\right) + \nu\nabla^2\underline{u} \,, \tag{2a}$$

$$\nabla \cdot \underline{u} = 0 \,. \tag{2b}$$

Here $\underline{\omega} = \nabla \times \underline{u}$ is the vorticity. The boundary condition at a wall is $\underline{u}|_{wall} = 0$. Other boundary conditions, such as periodicity or inflow-outflow, are imposed as appropriate.

The role of the pressure in incompressible flows is to enforce the continuity condition. This may be expressed formally by recalling that an arbitrary vector field $\underline{f}$ may be uniquely decomposed into a sum of a divergence-free field satisfying tangency at the boundary and the gradient of a potential,

$$\underline{f} = \underline{\psi} + \nabla\phi \,,$$

$$\nabla \cdot \underline{\psi} = 0 \qquad \underline{\psi} \cdot \underline{n}|_{wall} = 0 \,.$$

Let $\mathcal{P}$ be the projection operator that accomplishes this decomposition, that is,

$$\mathcal{P}\underline{f} = \underline{\psi} \,;$$

applying the projection operator $\mathcal{P}$ to equation (2a) we obtain

$$\frac{\partial \underline{u}}{\partial t} = -\mathcal{P}(\underline{\omega} \times \underline{u}) + \mathcal{P}(\nu\nabla^2\underline{u}) \,,$$

eliminating the dynamic pressure [15]. The above equation is the starting point for the numerical scheme described below.

Vector expansion method:

We write $\underline{u}$ as the expansion

$$\underline{u}(\underline{x},t) = \sum_{n=1}^{N} a_n(t)\underline{\psi}_n(\underline{x}) \ , \tag{3}$$

where each $\underline{\psi}_n$ satisfies

$$\nabla \cdot \underline{\psi}_n = 0 \ , \tag{4}$$

and the homogeneous boundary condition on $\underline{u}$. We need to derive a system of ODEs for the coefficients $a_n(t)(n = 1,2, \ldots,N)$. We do so by substituting the expansion (3) into (2a) and taking the inner product of the result with a set of weight vectors $\underline{\zeta}_m$ $(m = 1,2, \ldots,N)$ satisfying

$$\nabla \cdot \underline{\zeta}_m = 0 \tag{5}$$

and

$$\underline{\zeta}_m \cdot \underline{n}|_{wall} = 0 \ . \tag{6}$$

That is,

$$\int_V \underline{\zeta}_m(\underline{x}) \cdot [\text{momentum eq.}]dV = 0 \ , \quad m = 1,2, \ldots,N \ . \tag{7}$$

If the $\underline{\zeta}_m$ form a complete set and $N \to \infty$, this operation is equivalent to applying the projection operator because

$$\int_V \underline{\zeta}_m(x) \cdot \nabla\phi \ dV = -\int_V (\nabla \cdot \underline{\zeta}_m)\phi \ dV + \int_S \phi(\underline{\zeta}_m \cdot \underline{n})dS$$

$$= 0$$

for an arbitrary scalar field ϕ. An explicit representation of $\mathcal{P}$ may be given as

$$\mathcal{P}(\underline{f}) = \sum_{m,n} \underline{\zeta}_m Q_{mn}\langle\underline{\zeta}_n \cdot \underline{f}\rangle \ ,$$

where

$$Q_{mn} = \langle\underline{\zeta}_n \cdot \underline{\zeta}_m\rangle^{-1} \ .$$

The result of the computation given in (7) is the following system of ODEs:

$$A\dot{a} + \nu Ba = g \ , \tag{8}$$

where

$$A_{mn} = \int \underline{\zeta}_m \cdot \underline{\psi}_n \ dV \ , \tag{9}$$

$$B_{mn} = \int \underline{\zeta}_n \cdot (\nabla \times \nabla \times \psi_n)dV \ , \tag{10}$$

and g_m is quadratic in the a_n's,

$$g_m = -\int \zeta_m \cdot (\omega \times u)dV \ . \tag{11}$$

Thus, each evaluation of the $\dot{a}_n$'s requires the solution of a linear system and the computation of the nonlinear term. The choice of the vector functions ψ_n and ζ_m is crucial to the success of the method. Mathematically, of course, the sets $\{\psi_n\}$ and $\{\zeta_m\}$ must be complete in appropriate spaces of functions satisfying (4) plus boundary conditions and (5) and (6), respectively. From a computation standpoint we would like (1) rapid convergence of our expansions of u; (2) minimum (and ordered) coupling of the modes through the time-dependent and viscous operators, for example, banded structure for A and B; (3) efficient construction of the matrices A and B; and (4) efficient computation of the nonlinear term g.

In practice, the index n has three components, one for each spatial direction. The matrices A and B are diagonal in the homogeneous directions where Fourier series may be used but nondiagonal in the direction normal to the wall. For example, in the application to pipe flow described below, A and B are banded with the same number of bands. Thus, implicit treatment of the viscous term is possible at no extra cost.

Equation (8) is a complete statement of the dynamics. No extra equations are required to enforce boundary conditions or continuity, and no fractional time-steps are needed. In addition, the number of equivalent grid points in the computation is N/2. Thus, only two unknowns per mesh point are required because of the constraint (4) on the expansion vectors, allowing considerable savings in memory requirement.

For pipe flow [16] the boundary condition at the pipe wall $r = 1$ is $u(r = 1) = 0$. We assume periodic boundary conditions in the x-direction with period L and write the velocity field u as the expansion

$$u(r,\theta,x,t) = \sum_{n,k,\ell} a_{n,k,\ell}(t)\chi_n(r)\exp(ikx + i\ell\theta) \ , \tag{12}$$

where each expansion vector satisfies

$$\nabla \cdot [\chi_n(r)\exp(ikx + i\ell\theta)] = 0 \tag{13}$$

and

$$\chi_n(1) = 0 \ . \tag{14}$$

The weight vectors are given by

$$\zeta = \xi_m(r)\exp(-ikx - i\ell\theta) \ . \tag{15}$$

They are also divergence-free and satisfy the inviscid boundary condition,

$$\xi_m(1) \cdot \hat{e}_r = 0 \ . \tag{16}$$

[The (k,ℓ) dependence of χ_n and ξ_m is suppressed.] Applying the weighted residual method described above we find that for each wave vector (k,ℓ)

$$A\dot{a} + \frac{1}{Re} Ba = f \ , \tag{17}$$

where

$$A_{mn} = \int_0^1 \xi_m \cdot \chi_n r \, dr \ , \tag{18a}$$

$$B_{mn} = \int_0^1 \xi_m \cdot \widetilde{\nabla \times \nabla} \times \chi_n r \, dr \ , \tag{18b}$$

and

$$f_m = -\int_0^1 \underline{\xi}_m \cdot \left[\widetilde{\underline{\omega} \times \underline{u}} + 2\pi L \frac{dP}{dx} \hat{e}_x\right] r \, dr \ , \tag{18c}$$

and where $\sim$ denotes double-Fourier transformation in x and θ. Thus, except for the nonlinear term, the coupling of the equations occurs only through the radial modes as discussed above.

We find that the sequence of expansion vectors $\{\underline{\chi}_{-1}, \underline{\chi}_0^+, \underline{\chi}_0^-, \ldots, \underline{\chi}_n^+, \underline{\chi}_n^-, \ldots\}$ defined in the following satisfies the above requirements. For $n \geq 0$ the (r,θ,x) components are

$$\underline{\chi}_n^{\pm} = \begin{pmatrix} \chi_{n,r}^{\pm} \\ \chi_{n,\theta}^{\pm} \\ \chi_{n,x}^{\pm} \end{pmatrix} = \begin{pmatrix} \pm ikq_n^{\ell\pm1} \\ kq_n^{\ell\pm1} \\ \mp \frac{1}{r}\frac{d}{dr}(rq_n^{\ell\pm1}) - \frac{\ell}{r} q_n^{\ell\pm1} \end{pmatrix} \quad (k \neq 0) \ , \tag{19}$$

where

$$q_n^{\ell} = r^{|\ell|}(1 - r^2)^2 g_n^{(|\ell|)}(r^2) \qquad (n \geq 0) \tag{20}$$

and $g_n^{(\ell)}(y)$ is the shifted Jacobi polynomial [17],

$$g_n^{(\ell)}(y) = P_n^{(o,\ell)}(2y - 1) \ , \tag{21}$$

satisfying the orthogonality condition,

$$\int_0^1 y^{\ell} g_m^{(\ell)}(y) g_n^{(\ell)}(y) dy = C_m^2 \delta_{m,n} \ . \tag{22}$$

For $n = -1$ and $k \neq 0$, we use

$$\underline{\chi}_{-1} = \underline{\chi}_{-1}^{+} + \underline{\chi}_{-1}^{-} \ , \tag{23}$$

with $\underline{\chi}_{-1}^{\pm}$ given by (19) and

$$q_{-1}^{\ell} = r^{|\ell|}(1 - r^2) \ . \tag{24}$$

For the case $k = 0$, the above expansion vectors clearly are not complete and must be replaced by an alternative set. A convenient choice is given by $(n \geq 0)$,

$$\underline{\chi}_n^{-} = \begin{pmatrix} \frac{i\ell q_n^{\ell}}{r} \\ \frac{dq_n^{\ell}}{dr} \\ 0 \end{pmatrix} \quad \underline{\chi}_n^{+} = \begin{pmatrix} 0 \\ 0 \\ q_n^{\ell} \end{pmatrix} . \tag{25}$$

It is a simple matter to verify that the expansion vectors defined above yield the correct behavior of $\tilde{\underline{u}}(r,k,\ell)$ as $r \to 0$; for example, if $\ell > 0$,

$$\tilde{u}_r \to \gamma r^{\ell-1} ,$$

$$\tilde{u}_\theta \to i\gamma r^{\ell-1} ,$$

$$\tilde{u}_x \to \beta r^{\ell} ,$$

where γ and β are complex constants.

The completeness of the expansion is readily demonstrated. For example, if $k \neq 0$ and $\ell > 0$ we find from (19) that $1/2(\tilde{u}_r \pm i\tilde{u}_\theta)$ have the complete representation (and, thus, so do $\tilde{u}_r$ and $\tilde{u}_\theta$, separately),

$$\frac{1}{2}(\tilde{u}_r \pm i\tilde{u}_\theta) = \pm ika_{-1}r^{\ell\pm1}(1 - r^2) \pm ik \sum_{n\geq 0} a_n^{\pm} q_n^{\ell\pm1} , \tag{26}$$

where the first term on the right-hand side of each equation is used to satisfy a nonzero value of $d\tilde{u}_\theta/dr|_{r=1}$, that is, $(1/2)d\tilde{u}_\theta/dr|_{r=1} = -2ka_{-1}$, and the remaining sums are complete for complex functions having a double zero at the wall and satisfying $\tilde{u}_r \pm i\tilde{u}_\theta \to r^{\ell\pm1}$ as $r \to 0$. The $\tilde{u}_x$ component must satisfy the continuity constraint,

$$ik\tilde{u}_x + \frac{i\ell\tilde{u}_\theta}{r} + \frac{1}{r}\frac{d}{dr}(r\tilde{u}_r) = 0 , \tag{27}$$

which it does.

The corresponding weight vectors are essentially the curl of the χ's. More specifically, if $k \neq 0$ the weight vectors may be expressed as

$$\xi_m^{\pm} = \widetilde{\nabla \times \nabla} \times \begin{pmatrix} \mp iq_n^{\ell\pm1} \\ q_n^{\ell\pm1} \\ 0 \end{pmatrix} , \tag{28}$$

and the $\chi_n^{\pm}$ have the form

$$\chi_n^{\pm} = \widetilde{\nabla \times} \begin{pmatrix} -iq_n^{\ell\pm1} \\ \mp q_n^{\ell\pm1} \\ 0 \end{pmatrix} . \tag{29}$$

As a result, the (+) vectors are uncoupled from the (-) vectors. The resulting matrices A and B are nonadiagonal, except for an additional nonzero row and a column owing to the vector χ_{-1}. The limited bandwidth of the viscous matrix B results from the particular choice of the polynomials $g^{(\ell)}(y)$ given by (21). In particular, the Laplacian operator in the (r,θ) plane is equivalent to a tridiagonal matrix in the following sense:

$$\nabla^2[q_n^\ell(r)\exp(i\ell\theta)] = \left(\frac{1}{r}\frac{d}{dr}\, r\, \frac{d}{dr} - \frac{\ell^2}{r^2}\right) q_n^\ell(r)\exp(i\ell\theta)$$

$$= r^\ell[b_n^\ell g_{n-1}^{(\ell)}(r^2) + c_n^\ell g_n^{(\ell)}(r^2) + d_n^\ell g_{n+1}^{(\ell)}(r^2)]\exp(i\ell\theta) .$$

In [16] we applied the above technique to the problem of determining the time eigenvalues for linearized flow in a pipe and demonstrated exponential convergence of the expansion. The results of fully nonlinear calculations of axisymmetric structures are

shown in figures 5-7. The evolution of a corotating vortex structure is depicted in figure 5, in which azimuthal vorticity contours are shown. The term "corotating" indicates that the vorticity in the structure has the same sign as the mean flow vorticity. A counterrotating vortex structure is shown during various stages of its development in figure 6. The counterrotating structure has many features in common with the experimentally observed turbulent puff [18] — sharp trailing edge, cone-shaped leading edge, translation speed $\sim\bar{U}$ — but, unlike the experimental puff, which is self-sustaining, it decays in time. Clearly, three-dimensional simulations, presently under way, are required to capture this intriguing transitional flow structure on the computer. Nevertheless, the corotating and counterrotating vortex structures depicted appear to be important flow structures in more general axisymmetric pipe flow. As shown in figure 7, a random axisymmetric initial field evolves into a flow that is dominated by structures of these two types.

The above method has been applied successfully to channel flow and to flow between two concentric cylinders [19]. It seems clear that flow inside a spherical chamber and between concentric spheres could be attacked by the same technique, as well as flow in a curved pipe. External flows, such as flow past a cylinder or sphere, promise to be more challenging because the appropriate behavior at infinity must be incorporated into the expansion functions and because a rapidly convergent representation of the boundary-layer and wake regimes must be provided simultaneously.

In simple cases, the method can be generalized to the situation where walls are present in more than one coordinate direction. For example, in channel flow with square (y-z) cross section we might use the expansion vectors,

$$\underline{\psi}^{\pm} = \begin{pmatrix} \psi_x^{\pm} \\ \psi_y^{\pm} \\ \psi_z^{\pm} \end{pmatrix} = \begin{pmatrix} \pm q_m'(y)q_n'(z) - q_m'(y)q_n'(z) \\ \mp ikq_m(y)q_n'(z) \\ ik\bar{q}_m'(y)q_n(z) \end{pmatrix} e^{ikx} ,$$

where $q_\ell(s) = (1 - s^2)^2 P_\ell(s)$, and P_ℓ is a Legendre polynomial leading to block-banded d/dt and viscous matrices with each component matrix banded. For completely arbitrary geometries, it appears that expansion in global basis functions satisfying continuity and the boundary conditions would be cumbersome. In that case, using finite-element expansions with discontinuities in some derivative might be the way to proceed [20].

LOW-ORDER EXPANSIONS OF A TURBULENT FIELD

In the above examples, solutions of the Navier-Stokes equations representing turbulent flows are computed by essentially tracking the evolution of a point in the (N^3) dimensional state-space of the coefficients where N is ≈ 100 for low Reynolds numbers. Can we, by cleverly choosing our basis functions, reproduce the same flow (viz., any desired statistic of the flow to within some accuracy) in a much lower dimensional phase space? In other words, is the attractor in the $O(10^6)$ space of much lower dimension? The answer is probably yes, but we do not yet know how to find these basis functions except for some special cases. For example, if the vorticity is concentrated into a small region of physical space we achieve a significant reduction in the dimension of coefficient space by tracking vorticity in Lagrangian coordinates [21]. For example, one can reproduce the oscillation of a slightly elliptical vortex tube with less than a hundred points around the tube. Yet the vortex has a rich energy spectrum, as shown in figure 8. Figure 9 shows the three-dimensional wake of a sphere represented by ≈ 500 points in 10-15 computational vortex filaments [22].

If the structure within the vortex tube is an important aspect of the dynamics, then several computational filaments must be used to represent the physical vortex tube. Ashurst [23] has demonstrated the instability of a vortex ring using this technique. The instability of a vortex tube to localized twisting of the vortex lines representing varying axial flow within the tube is shown in figure 10. See Nakamura et al. [24] for more examples in this area, including examples of vortex breakdown. Chorin [25] has studied the statistics of high-Reynolds-number turbulent flow using similar methods.

In the general setting, where vorticity fills a significant portion of the domain, Lagrangian vortex methods lose their advantage, requiring as many points as traditional Eulerian methods. In this case, the large-eddy simulation (LES) technique [26] is an attractive alternative. In LES, one solves the space-filtered Navier-Stokes equations on a relatively coarse mesh for the evolution of the large eddies of the turbulent flow. The equations contain subgrid-scale stress terms that must be modeled. The method has proved quite successful in a variety of applications (see, for example, the LES technique applied to channel flow by Moin and Kim [27]) and one can save a large fraction of the grid points required to do a direct simulation of the same flow. Even so, it appears that one and a half to two decades of scale in each direction (especially if walls are present), or a total of half a million points, are needed to represent the important energy-containing eddies.

Clearly it would be advantageous if we could represent, say, turbulent channel flow with approximately 100 interacting flow structures, each structure depending parametrically on a few time-dependent coefficients. The dynamics would be given by coupled nonlinear ODEs for the coefficients. As pointed out by Saffman [28], the idea of building a turbulent field out of a collection of predetermined or organized structures is not new. Forty years ago Synge and Lin [29] proposed a representation of isotropic turbulence by a (random) superposition of Hill spherical vortices. But this idea was used only as a kinematic description of turbulence. For it to become a full dynamical description of an evolving turbulent flow, one needs equations of motion for the parameters of the vortices — position, orientation, size, strength — that accurately represent the dynamics of the Navier-Stokes equations. Even if these equations of motion were derived, it appears doubtful that only a few hundred such vortices would be required to accurately represent a general turbulent flow.

An analogous situation occurs for the one-dimensional Burgers' equation where exact dynamical equations are known for the "pole" decomposition of the solution field [30]. In this case, the solution to

$$\frac{\partial u}{\partial t} + u \frac{\partial u}{\partial x} = \nu \frac{\partial^2 u}{\partial x^2} \tag{30}$$

can be represented by

$$u(x,t) = -2\nu \sum_{n=1}^{N} \frac{1}{x - z_n(t)} , \tag{31}$$

where the z_n are complex and satisfy the ODEs

$$\frac{dz_n}{dt} = -2\nu \sum_{\substack{m=1 \\ m \neq n}}^{N} \frac{1}{z_n - z_m} . \tag{32}$$

For real solutions $u(x,t)$ the z_n must come in complex conjugate pairs. Thus, each flow structure is given by

$$\frac{-4\nu(x - \mathrm{Re}\ z)}{(x - \mathrm{Re}\ z)^2 + (\mathrm{Im}\ z)^2} , \tag{33}$$

which depends on the complex parameter z. However, it appears that the number of structures (33) required to reproduce an arbitrary initial field is proportional to the ratio of the largest to smallest scale of that field. So although the pole decomposition in one-dimensional Burgers' flow has some of the features we are looking for in our flow-structure representation of three-dimensional Navier-Stokes flow — exact or approximate equivalence to a system of ODEs for the structure parameters — it has the undesirable feature that we wish to avoid in three dimensions — the large number of structures required to represent an arbitrary flow field.

SUMMARY

The computer simulation of turbulent flows is a challenging numerical problem. Because the three-dimensional turbulent flow field has a wide range of scales with chaotic behavior, one looks for rapidly convergent spatial representations of these fields to minimize the number of ODEs in the time required. In this context, spectral expansions appear to be a powerful tool but special attention must be paid to minimize the work caused by coupling of the resultant ODEs. A number of low-Reynolds-number homogeneous flows have been computed, using meshes with up to 128^3 points; they have produced significant results for understanding turbulence and important information for turbulence modelers. We expect results from the direct simulation of wall-bounded turbulent flows in the near future, using spectral expansions. In this case, further difficulties arise because of the presence of the no-slip condition and the fact that there is a minimum Reynolds number, of the order of a few thousand, to sustain turbulence. For these flows, expansion of the velocity field in terms of divergence-free vectors satisfying the no-slip condition appears particularly promising.

In any event, the direct simulation technique will continue to strain computational resources and thereby remain a research tool. More practical low-order expansion techniques, such as large-eddy simulation and vortex methods, have already made significant contributions and will continue to be improved as modeling becomes more sophisticated. It is hoped that eventually modeling will evolve such that only a few hundred computational flow structures are required to represent a complex turbulent flow.

ACKNOWLEDGMENT

The author wishes to thank Dr. John Kim for comments on a draft of this paper and Dr. Parviz Moin and Mr. Morris Rubesin for many helpful discussions.

REFERENCES

[1] - J. von Neumann: "Recent Theories of Turbulence," 1949 report to the Office of Naval Research, reprinted in John von Neumann, Collected Works, Vol. VI, A. H. Taub, ed., Macmillan Co., New York, 1963, pp. 437-472.

[2] - H. W. Emmons: "The Numerical Solution of the Turbulence Problem," in Proceedings of Symposia in Applied Mathematics, Vol. I, McGraw-Hill, New York, 1949, pp. 67-71.

[3] - J. W. Deardorff: "A Numerical Study of Three-Dimensional Turbulent Channel Flow at Large Reynolds Numbers," J. Fluid Mech., Vol. 41, 1970, pp. 453-480.

[4] - S. A. Orszag and G. S. Patterson, Jr.: "Numerical Simulation of Three-Dimensional Homogeneous Isotropic Turbulence," Phys. Rev. Lett., Vol. 28, 1972, pp. 76-79.

[5] - G. K. Batchelor: "The Theory of Homogeneous Turbulence," Cambridge University Press, Cambridge, 1967.

[6] - J. O. Hinze: "Turbulence," 2nd ed., McGraw-Hill Inc., New York, 1975, p. 722.

[7] - J. Laufer: "The Structure of Turbulence in Fully Developed Pipe Flow," NACA 1174, 1954.

[8] - C. J. Lawn: "The Determination of the Rate of Dissipation in Turbulent Pipe Flow," J. Fluid Mech., Vol. 48, 1971, pp. 477-505.

[9] - H. P. Bakewell, Jr. and J. L. Lumley: "Viscous Sublayer and Adjacent Wall Region in Turbulent Pipe Flow," Phys. Fluids, Vol. 10, 1967, pp. 1880-1889.

[10] - D. Coles: "Prospects for Useful Research on Coherent Structure in Turbulent Shear Flow," Proc. Indian Acad. Sci. (Engg. Sci.), Vol. 4, 1981, pp. 111-127.

[11] - P. Moin: "Numerical Simulation of Wall-Bounded Turbulent Shear Flows," Proceedings of the 8th International Conference on Numerical Methods in Fluid Dynamics, June 28-July 2, 1982, Aachen, W. Germany, Springer-Verlag, New York, 1983, pp. 55-76.

[12] - R. S. Rogallo: "Numerical Experiments in Homogeneous Turbulence," NASA TM-81315, 1981.

[13] - J. L. Lumley and G. R. Newman: "The Return to Isotropy of Homogeneous Turbulence," J. Fluid Mech., Vol. 82, 1977, pp. 161-178.

[14] - S. A. Orszag: "Spectral Methods for Problems in Complex Geometries," J. Comp. Phys., Vol. 37, 1980, p. 70.

[15] - A. J. Chorin and J. E. Marsden: "A Mathematical Introduction to Fluid Mechanics," Springer-Verlag, New York, 1979.

[16] - A. Leonard and A. Wray: "A New Numerical Method for the Simulation of Three-Dimensional Flow in a Pipe," Proceedings of the 8th International Conference on Numerical Methods in Fluid Dynamics, June 28-July 2, 1982, Aachen, W. Germany, Springer-Verlag, New York, 1983, pp. 335-342.

[17] - M. Abramowitz and I. A. Stegun, editors: "Handbook of Mathematical Functions," National Bureau of Standards Applied Mathematics Series-55, Sec. 22, U.S. Government Printing Offices, Washington, D.C., 1968.

[18] - I. Wygnanski, M. Sokolov, and D. Friedman: "On Transition in a Pipe. Part 2. The Equilibrium Puff," J. Fluid Mech., Vol. 69, 1975, pp. 283-304.

[19] - R. D. Moser, P. Moin, and A. Leonard: "A Spectral Method for the Navier-Stokes Equations with Applications to Taylor-Couette Flow," submitted to J. Comp. Phys.

[20] - J. Donea, S. Giuliani, H. Laval, and L. Quartapelle: "Solution of the Unsteady Navier-Stokes Equations by a Finite-Element Projection Method," in Computational Techniques in Transient and Turbulent Flow, Vol. 2, C. Taylor and K. Morgan, eds., Pineridge Press, Swansea, 1981.

[21] - A. Leonard: "Vortex Methods for Flow Simulation," J. Comp. Phys., Vol. 37, 1980, pp. 289-335.

[22] - A. Leonard: "Simulation of Three-Dimensional Separated Flows with Vortex Filaments," in Lecture Notes in Physics No. 59, Springer-Verlag, New York, 1976, pp. 280-284.

[23] - W. T. Ashurst: "Vortex Ring Instability," Bull. Amer. Phys. Soc., Vol. 26, No. 9, 1981, p. 1267.

[24] - Y. Nakamura, A. Leonard, and P. R. Spalart: "Numerical Simulation of Vortex Breakdown by the Vortex Filament Method," Proceedings of the AGARD Symposium on Aerodynamics of Vortical Type Flows in Three Dimensions, Rotterdam, The Netherlands, April 25-27, 1983 (to appear).

[25] - A. J. Chorin: "The Evolution of a Turbulent Vortex," Commun. Math. Phys., Vol. 83, 1982, pp. 517-535.

[26] - J. H. Ferziger: "Large Eddy Numerical Simulation of Turbulent Flow," AIAA J., Vol. 15, 1977, p. 1261.

[27] - P. Moin and J. Kim: "Numerical Investigation of Turbulent Channel Flow," J. Fluid Mech., Vol. 118, 1982, pp. 341-377.

[28] - P. G. Saffman: "Coherent Structures in Turbulent Flow," in Lecture Notes in Physics No. 136, Springer-Verlag, New York, 1981, pp. 1-9.

[29] - J. L. Synge and C. C. Lin: "On a Statistical Model of Isotropic Turbulence," Trans. Roy. Soc. Canada, Sec. III, 1943, pp. 45-79.

[30] - D. V. Choodnovsky and G. V. Choodnovsky: "Pole Expansions of Nonlinear Partial Differential Equations," Nuovo Cimento, Vol. 40B, 1977, pp. 339-353.

TABLE 1.- MESH-POINT REQUIREMENTS

Reynolds number	Kolmogorov length		Number of mesh points ($\Delta = 2\eta$)
	η/D	η^+ wall units	$N = \frac{10\pi}{4}\left(\frac{D}{\Delta}\right)^3$
5×10^3	0.0045	1.6	1.0×10^7
1×10^4	0.0028	1.8	4.3×10^7
5×10^4	0.00093	2.4	1.2×10^9
1×10^5	0.00058	2.8	5.1×10^9
5×10^5	0.00019	3.8	1.5×10^{11}

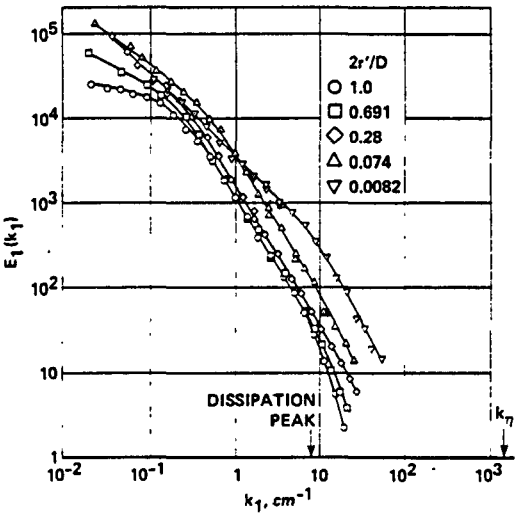

Figure 1.- One-dimensional velocity spectra in a pipe. Re = 500,000; r' is distance from pipe wall. Dissipation peak is approximate location of $\max\{k_1^2 E_1(k_1)\}$; k_η is Kolmogorov wave number (from Laufer [7]).

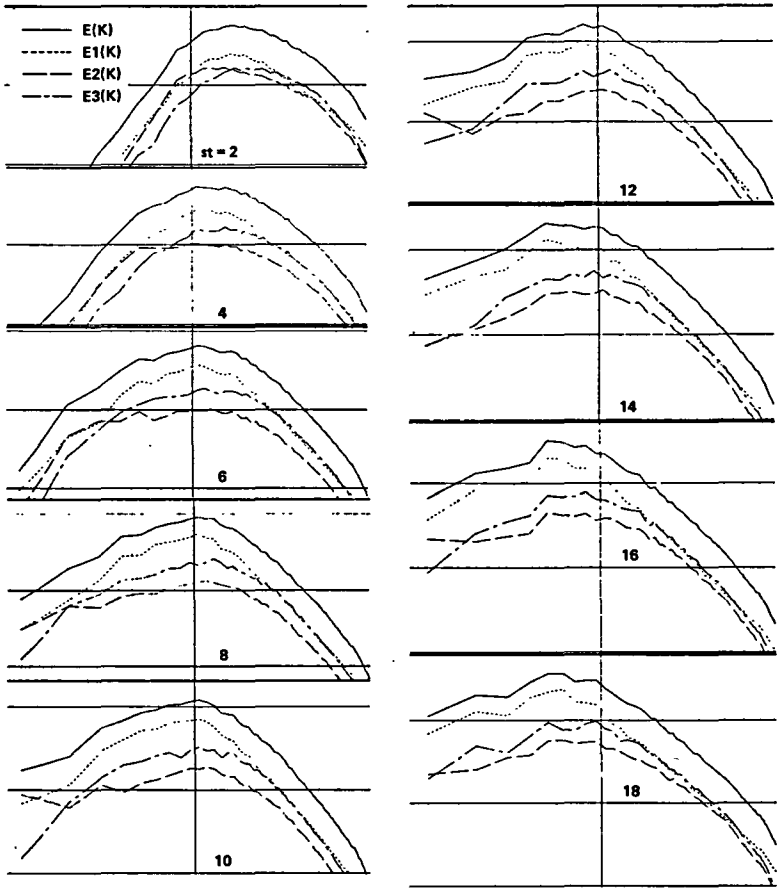

Figure 2.- Three-dimensional energy spectra for homogeneous shear turbulence; $L_{11,1}$ is the integral scale in the streamwise direction; experiments cited: TC, S. Tavoularis and S. Corrsin, J. Fluid Mech., Vol. 104, pp. 311-347, 1981; F. H. Champagne, V. G. Harris, and S. Corrsin, J. Fluid Mech., Vol. 41, pp 81-139, 1970 (from Rogallo [12]).

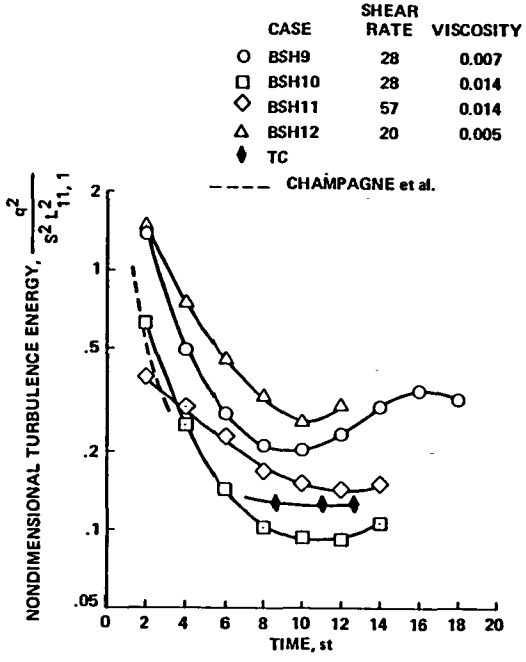

Figure 3.- The tendency toward equilibrium of the turbulence and shear time scales for homogeneous shear turbulence (from Rogallo [12]).

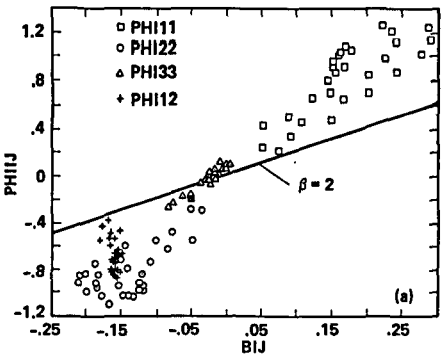

(a) Correlation between tensor ϕ_{ij} and tensor b_{ij} in homogeneous shear turbulence (from Rogallo [12]).

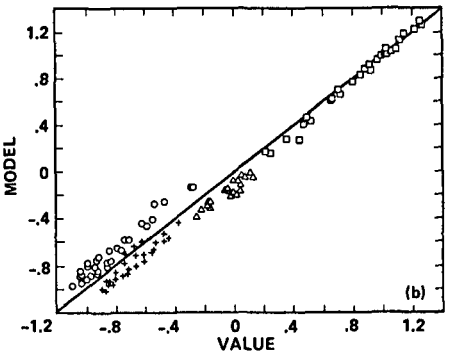

(b) Comparison of measured (ϕ_{ij}) and modeled (βb_{ij}) terms (from Rogallo [12]).

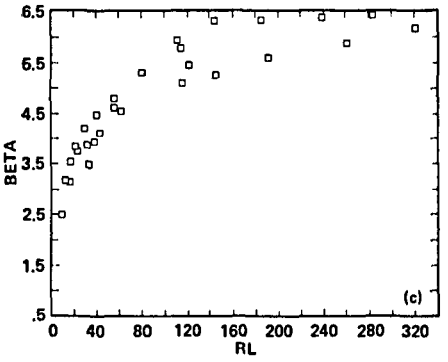

(c) Variation of model coefficient with Reynolds number, $R_L = qL_{11,1}/\nu$ (from Rogallo [12]).

Figure 4.- Modeling of the tensor ϕ_{ij}.

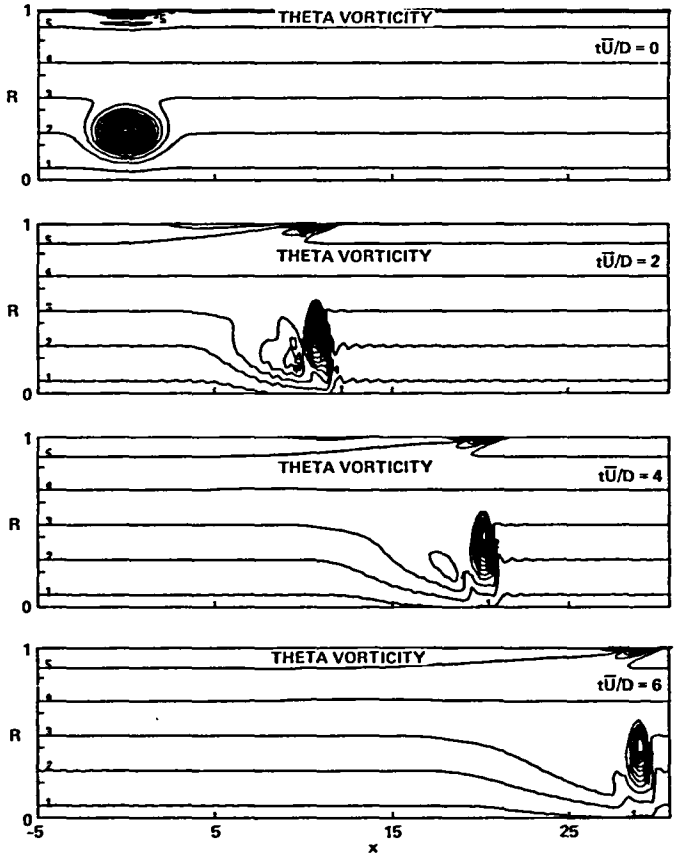

Figure 5.- Evolution of a corotating vortex in pipe flow. Contours of azimuthal vorticity; radial scale expanded by a factor of 10; Re = 2200; mean flow is from left to right.

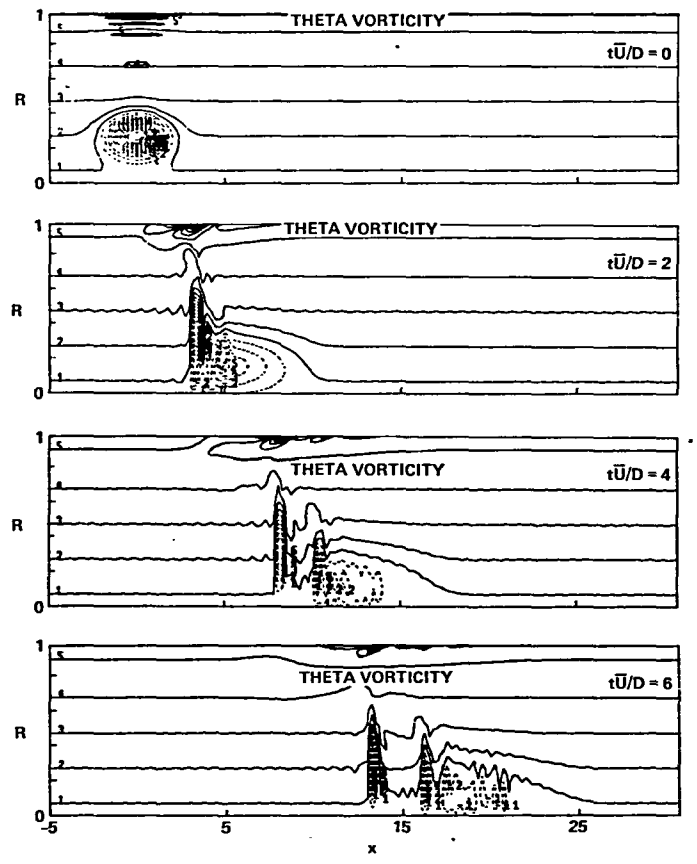

Figure 6.- Evolution of a counterrotating vortex in pipe flow.

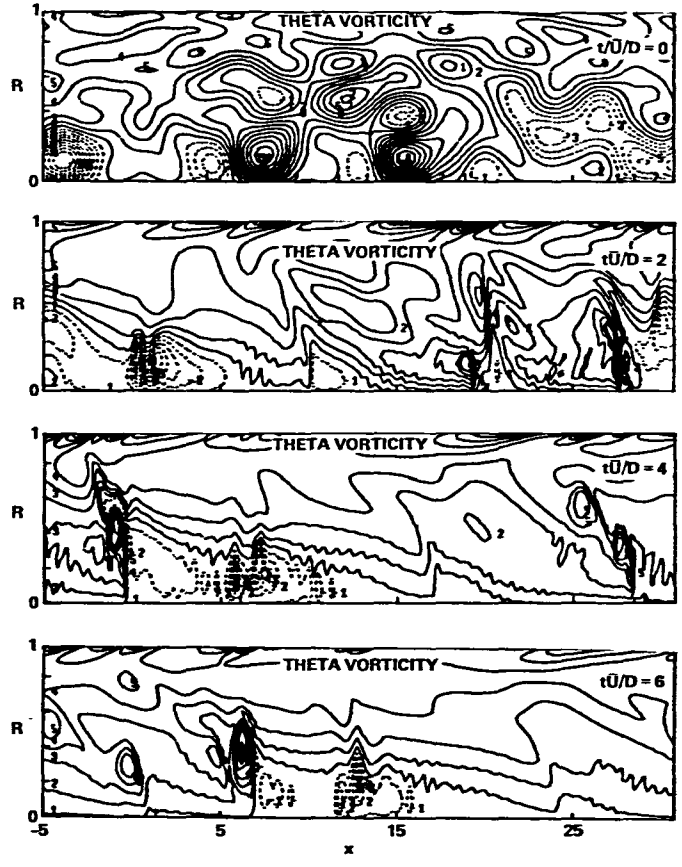

Figure 7.- Evolution of a random axisymmetric field in pipe flow.

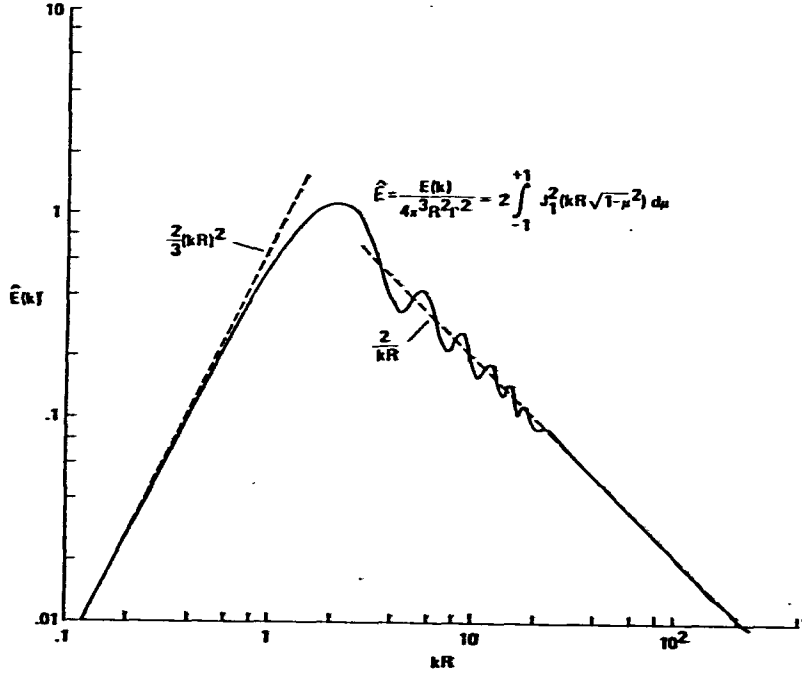

Figure 8.- Three-dimensional energy spectrum of a ring vortex; R is ring radius; Γ is circulation; vortex core radius is zero.

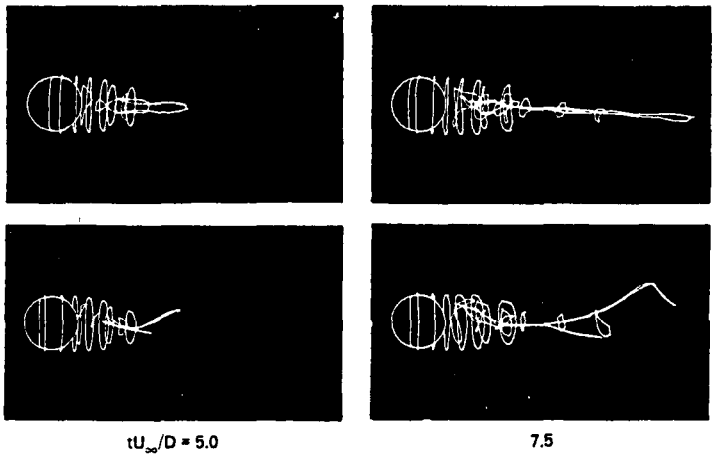

Figure 9.- Vortex simulation of flow past a sphere with an impulsive start as observed from two directions perpendicular to one another (from Leonard [22]).

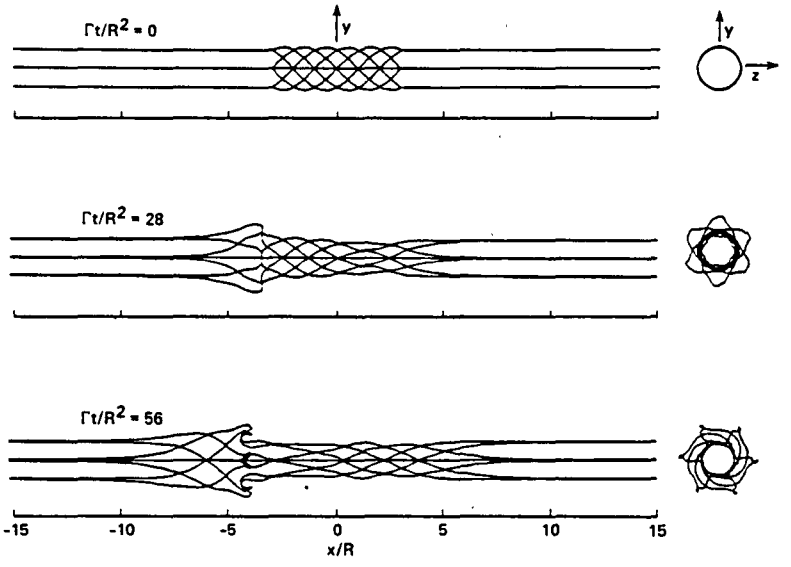

Figure 10.- Vortex simulation of the instability of a tube of vorticity because of localized twisting of the vortex lines.

1. Report No.	2. Government Accession No.	3. Recipient's Catalog No.
NASA TM-84320		

4. Title and Subtitle	5. Report Date
NUMERICAL SIMULATION OF TURBULENT FLUID FLOWS*	February 1983
	6. Performing Organization Code
7. Author(s)	8. Performing Organization Report No.
A. Leonard	A-9206
	10. Work Unit No.
9. Performing Organization Name and Address	T-6465
NASA Ames Research Center Moffett Field, Calif. 94035	11. Contract or Grant No.
	13. Type of Report and Period Covered
12. Sponsoring Agency Name and Address	Technical Memorandum
National Aeronautics and Space Administration Washington, D.C. 20546	14. Sponsoring Agency Code 505-31-21-01-00-21

15. Supplementary Notes *Presented at the Symposium on Numerical Methods in Engineering Science, Paris, France, March 14-16, 1983.
Point of Contact: A. Leonard, Ames Research Center, MS 202A-1, Moffett Field, Calif. 94035, (415)965-6459 or FTS 448-6459.

16. Abstract

Recent developments in the numerical simulation of turbulent flows are discussed. This limited survey covers computational requirements for the direct simulation of turbulence, simulation of arbitrary homogeneous flows, a new expansion technique for wall-bounded flows with application to pipe flow, and possibilities of flow representations or modeling techniques that allow the simulation of high-Reynolds-number flows with a relatively small number of dependent variables.

17. Key Words (Suggested by Author(s))	18. Distribution Statement
Fluid dynamics Computational Turbulence Numerical simulation	Unlimited Subject Category - 34

19. Security Classif. (of this report)	20. Security Classif. (of this page)	21. No. of Pages	22. Price*
Unclassified	Unclassified	22	A02

*For sale by the National Technical Information Service, Springfield, Virginia 22161